Available online at www.sciencedirect.com
SCIENCE DIRECT
Geochimica et Cosmochimica Acta 70 (2006) 2957–2969
Geochimica
www.elsevier.com/locate/gca

Restructuring of polygalacturonate on alumina upon hydration—Effect on phosphate sorption kinetics

Christian Mikutta [a,*], Jaane Krüger [a], Gabriele E. Schaumann [b], Friederike Lang [a]

[a] Department of Soil Science, Institute of Ecology, Berlin University of Technology, Salzufer 12, D-10587 Berlin, Germany
[b] Department of Environmental Chemistry, Institute of Environmental Technology, Berlin University of Technology, Straße des 17. Juni 135, D-10623 Berlin, Germany

Received 5 December 2005; accepted in revised form 20 March 2006

Abstract

Hydration of organic coatings in soils is expected to affect the sorption of oxyanions onto hydrous Fe and Al oxides. We hypothesized that the hydration of polygalacturonate (PGA) coatings on alumina (Al_2O_3) increases their permeability for phosphate. Pure and PGA-coated alumina were equilibrated in deionized water for 2 and 170 h at pH 5 and 20 °C before studying (i) their porosity with N_2 gas adsorption and ^1H NMR relaxometry, (ii) structural changes of PGA-coatings with differential scanning calorimetry (DSC), and (iii) the kinetics of phosphate sorption and PGA desorption in batch experiments. Scanning electron micrographs revealed that PGA molecules formed three-dimensional networks with pores ranging in size from <10 to several hundred nanometers. Our NMR results showed that the water content of intraparticle alumina pores decreased upon PGA sorption, indicating a displacement of pore water by PGA. The amount of water in interparticle alumina pores increased strongly after PGA addition, however, and was attributed to water in pores of PGA and/or in pores at the PGA-alumina interface. The flexibility of PGA molecules and the fraction of a PGA gel phase increased within one week of hydration, implying restructuring of PGA. Hydration of PGA coatings increased the amount of phosphate defined as instantaneously sorbed by 84%, showing that restructuring of PGA enhanced the accessibility of phosphate to external alumina surfaces. Despite the fact that the efficacy of phosphate to displace PGA was higher after 170 h than after 2 h, a higher phosphate surface loading was required after 170 h to set off PGA desorption. Our findings imply that the number of PGA chain segments directly attached to the alumina surface decreased with time. We conclude that hydration/dehydration of polymeric surface coatings affects the sorption kinetics of oxyanions, and may thus control the sorption and transport of solutes in soils.
© 2006 Elsevier Inc. All rights reserved.

1. Introduction

In soils and sediments minerals are partially covered with organic matter (Heil and Sposito, 1995; Ransom et al., 1997; Mayer and Xing, 2001; Gerin et al., 2003; Kaiser and Guggenberger, 2003). Under field and laboratory conditions, organic matter is subjected to moisture fluctuations that may change its physico-chemical properties due to interaction with water molecules (LeBoeuf and Weber, 2000; Schaumann et al., 2000; Schaumann, 2005; Schaumann and LeBoeuf, 2005). Hydration-induced changes in the macromolecules' mobility (Schaumann and LeBoeuf, 2005) may affect the retention of nutrients and pollutants by minerals coated with organic matter. The ability of soils and soil organic matter to sorb or release organic pollutants has been shown to depend on the state of hydration, hydration time, wetting and drying cycles, and the water content of the samples (Gaillardon, 1996; Altfelder et al., 1999; Johnson et al., 1999; Schaumann et al., 2004). In addition, the structure of organic matter can be affected by the dehydration technique applied in the laboratory, e.g., prior to sorption experiments (Altfelder et al., 1999). For example, structural changes of organic matter upon freeze-drying have been reported (Wedlock et al., 1983; Jouppila and Roos, 1997; Allison et al., 1998; Souillac et al., 2002). The hydration/dehydration-induced change of molecular structures of organic matter is therefore

* Corresponding author. Fax: +49 30 314 73 548.
E-mail address: christian.mikutta@tu-berlin.de (C. Mikutta).

0016-7037/$ - see front matter © 2006 Elsevier Inc. All rights reserved.
doi:10.1016/j.gca.2006.03.007

expected to affect the transport of solutes like hydrophobic pollutants through organic matter of soils and sediments (Brusseau and Rao, 1989; Pignatello and Xing, 1996; Cornelissen et al., 1998).

It has been suggested that soil organic matter (SOM) consists of rubbery (more flexible) and glassy (less flexible) domains (LeBoeuf and Weber, 1997) as known for synthetic polymers. The glass transition temperature, T_g, marks the temperature at which a glassy matrix becomes rubbery (Young and Lovell, 1991), and is a function of the side chain mobility in macromolecules. Usually, the incorporation of water molecules into the polymeric framework of isolated humic substances, soil and peat samples upon hydration reduces T_g, i.e., plasticizes polymer matrices (LeBoeuf and Weber, 1997; Schaumann and Antelmann, 2000; Schaumann and LeBoeuf, 2005).

It has been found by differential scanning calorimetry (DSC) and ^{1}H NMR-relaxometry analyses that peat or humus-rich soil samples exhibit first-order swelling kinetics upon hydration with time constants (reciprocal rate constants) of up to 6 days (Schaumann et al., 2004, 2005; Schaumann and LeBoeuf, 2005). Changes in proton relaxation times upon swelling of organic matter depend on the pore size distribution initially present in organic samples and on the quality of the organic material studied (Schaumann et al., 2004): while swelling of starch led to an increase in proton relaxation times, swelling of semolina or organic matter in peat and soil samples generally reduced the relaxation times (Schaumann et al., 2004, 2005). These effects were interpreted as an increase in intraparticle pore size and a decrease in interparticle pore size of organic matter upon water absorption (Schaumann et al., 2004, 2005).

Swelling of mineral-associated polymers through the incorporation of water molecules into the polymer structure might affect the sorption of oxyanions like phosphate or arsenate to Fe and Al oxides. An increase in intraparticle pore size of organic matter voids upon swelling of organic matter in conjunction with an increased mobility of polymer chains upon hydration might facilitate the Brownian motion and Fickian diffusion through more flexible (rubbery) polymer domains and hence favor the fast sorption of oxyanions. However, a decrease in interparticle pore size of sorbed organic matter upon swelling might reduce the accessibility of mineral surfaces to oxyanions.

The objective of this study was therefore to test whether the slow swelling of polymers sorbed to Fe and Al oxides affects phosphate sorption kinetics. Specifically, we hypothesized that the hydration of polygalacturonate (PGA) coatings on alumina (Al_2O_3) increases their permeability for phosphate. We used PGA as a well-defined model substance for the gelatinous mucilage covering the root apices of many plant species (Knee et al., 2001). Mucilage exuded by plant's root caps is confined to the soil–root interface because mucilage components diffuse very slowly into the soil (Rovira, 1969; Sealey et al., 1995). Mucilage of maize plants consists of 90–95% polysaccharides with about 20–35% of uronic acids (Cortez and Billes, 1982; Morel et al., 1986), and is susceptible to swelling due to water absorption (e.g., Guinel and McCully, 1986). At the soil–root interface the cycling of nutrients is therefore likely to be influenced by the state of hydration of organic coatings made up of macromolecular root exudates.

2. Materials and methods

2.1. General approach

We used alumina as a non-paramagnetic high-surface-area model adsorbent that could be used for ^{1}H NMR measurements. Pure and PGA-coated alumina samples were saturated in doubly deionized water at pH 5 for 2 and 170 h. After each equilibration time, phosphate sorption experiments were performed. Similarly, changes in pore size distribution were then monitored with ^{1}H NMR relaxometry and N_2 gas adsorption at 77 K. Differential scanning calorimetry (DSC) was used to identify changes in the molecular structure of sorbed PGA molecules upon hydration for 2 and 170 h, respectively. Details of the methods used are described in the following sections.

2.2. Preparation of organic coatings

The activated, weakly acid alumina (type 506-C-I) was purchased from Aldrich (Sigma–Aldrich Chemie GmbH). The mesoporous alumina had a particle size of 150 mesh (<105 μm) and an average pore size of 5.8 nm (Aldrich). Polygalacturonic acid (P81325, $(C_6H_8O_6)_n$, >95%, M = 25–50 kDa) was purchased from Fluka (Sigma–Aldrich Chemie GmbH) and comprised 37.2% C and 0.05% N (Elementar Vario EIII C/N/S Analyzer). The PGA contained negligible amounts of polyvalent cations with Ca being the most dominant with 5.7 mmol kg^{-1}. The content of paramagnetic Mn and Fe species was below 0.3 mmol kg^{-1}. Polygalacturonate solutions were prepared by dissolving polygalacturonic acid in 0.01 M KNO_3 solutions with the addition of 10 μL of 1 M KOH mg^{-1} PGA. Afterwards, the pH of the solutions was adjusted to pH 5 using 0.01 M HNO_3 without any visible flocculation occurring.

We followed a standardized procedure in order to prepare PGA coatings on alumina prior to our ^{1}H NMR, DSC, and phosphate sorption experiments. This procedure ensured comparability between experimental results of different methodologies.

To disperse alumina and hydrate adsorption sites, 7.5 g alumina were weighed into a 1-L PE bottle and shaken in 10 mL 0.01 M KNO_3 background electrolyte (pH 5) for 24 h on a reciprocating shaker (85 rev min^{-1}). Subsequently, either 990 mL of 0.01 M KNO_3 solution containing 1515 mg PGA-C L^{-1} (pH 5) or 990 mL of background electrolyte solution (pH 5) were added. The PGA solution also contained 5 μM $AgNO_3$ to impair microbial activity. The pH was maintained at 5 ± 0.02 using dilute HNO_3. After 24 h, the suspension was repetitively centrifuged at 5500g for 20 min and washed with 500 mL doubly deion-

ized water until the total organic C (TOC) concentration in the supernatant solution of PGA-treated alumina was negligible (<5 mg C L^{-1}, Shimadzu TOC-5050A Autoanalyzer). After determination of the gravimetric water content, the samples were immediately used for subsequent analyses (^{1}H NMR, DSC, and phosphate sorption). In all experiments, the gravimetric water content of pure and PGA-coated alumina was $42 \pm 1\%$ and $60 \pm 1\%$, respectively. Because the water content is a crucial parameter in the DSC analysis and highly variable at small scale, we additionally determined the water content of the individual samples used for DSC analysis (see Section 2.5). A part of the pure and C-coated alumina was freeze-dried for total organic C determinations and N_2 adsorption measurements. Freeze-drying was accomplished after freezing the samples at −80 °C in a Christ α 2–4 freeze drier (Osterode, Germany). In addition, the freeze-dried samples were examined by scanning electron microscopy (Hitachi S-4000) after the samples had been surface sputtered with Au (~5 nm Au layer thickness).

To test the influence of hydration time on porosity, organic matter quality, and phosphate sorption, samples were stored (non-agitated) in the dark at 20 °C at pH 5 for 2 and 170 h, respectively.

2.3. Nitrogen adsorption

Specific surface area and porosity were determined with a Quantachrome Autosorb-1 automated gas sorption system (Quantachrome, Syosset, NY). Approximately 100 mg pure and PGA-coated alumina were degassed until the increase of pressure rate by vapor evolution was below about 1.3 Pa min^{-1} within a 0.5-min test interval. Helium was used as a backfill gas. We used 79-point N_2 adsorption and desorption isotherms from 1.0×10^{-5} to 0.995 P/P_0. Specific surface area was calculated from the BET equation (Brunauer et al., 1938). Micropore (<2 nm) volume and average micropore diameter were determined according to the Dubinin-Radushkevic method (Gregg and Sing, 1982). The mesopore (2–50 nm) size distribution was calculated from the adsorption leg using the BJH method (Barrett et al., 1951). Total pore volume was taken at 0.995 P/P_0 and the average pore diameter was calculated as $D_p = 4\ V_{liq}/SSA$, where V_{liq} is the volume of liquid N_2 contained in pores at 0.995 P/P_0, and SSA is the BET surface area. All isotherms were recorded in triplicate.

2.4. ^{1}H NMR relaxometry

We used ^{1}H NMR relaxometry to determine changes in pore size distribution of water-saturated pure and PGA-coated alumina samples. The principle of ^{1}H NMR relaxometry has been described elsewhere (Kenyon, 1992, 1997; Schaumann et al., 2004, 2005). Triplicate samples of moist pure and PGA-coated alumina (~20 g) were weighed into 50-mL centrifuge tubes (Nalgene, polypropylene). The gravimetric water content of pure and PGA-coated alumina was $42 \pm 1\%$ and $60 \pm 1\%$, respectively. The samples were allowed to equilibrate in a climate-controlled room at 20 °C. The ^{1}H NMR relaxation experiments were performed 2 and 170 h after PGA sorption. The measurements were conducted on a 2 MHz relaxometer at a magnetic flux density of 0.047 T (Maran 2, Resonance Instruments, UK.). We used the Carr-Purcell-Meiboom-Gill (CPMG, 90°-τ-180°) pulse sequence with 4096 recorded echoes, a 150-μs echo spacing τ and a 1.2-s delay time. The scans were stacked 512 times. Provided that (i) water protons in porous media are in the fast diffusion limit (Brownstein and Tarr, 1979) and (ii) relaxation coming from the presence of paramagnetic materials is negligible, the transversal relaxation time constant T_2 is related to the relaxation time constant of the bulk water, the transversal surface relaxivity, and the pore size (Kenyon, 1992, 1997; Hinedi et al., 1997; Straley et al., 1997):

$$1/T_2 = 1/T_{2b} + \rho_2 SA/V = 1/T_{2b} + \rho_2 m/D_p, \quad (1)$$

where T_2 is the measured transversal relaxation time constant of water in a porous medium (s), T_{2b} is the bulk relaxation time constant of water at infinite distance from the pore walls (s), m is a shape factor, which is four assuming cylindrical pore geometry (Hinedi et al., 1997), D_p is the pore size (m), ρ_2 is the transversal surface relaxivity that parameterizes the strength of the surface relaxation (m s^{-1}), SA is the internal surface area (m^2), V is the volume of water contained in pores of the sample (m^3).

Using the inverse algorithm implemented in the WinDXP software package (Resonance Instruments Ltd., UK), we fitted the magnetization decay curves with a sum of exponential decay curves using 128 time constants between 0.1 and 6000 ms to calculate robust T_2 distributions. To ensure comparability between pure and PGA-coated alumina, the T_2 time constant distributions of each adsorbent were normalized to the mass of alumina present in the sample. This was done because in the PGA-coated alumina samples 31% less water-filled alumina pores were present compared to the pure alumina samples. Additionally, the relaxation decays, $M(t)$, monitored during application of the CPMG pulse sequence were normalized to their amplitude and fitted to a sum of three exponential decay functions:

$$M(t) = F_1 \exp(-t/T_{2-1}) + F_2 \exp(-t/T_{2-2}) + F_3 \exp(-t/T_{2-3}), \quad (2)$$

where F_i is the fraction of water held in the ith pore domain, and T_{2-i} are the respective transversal relaxation time constants (s) of water relaxing in the i-th pore water domain, and t is time (s). Coefficients of determination of the fits were always $\geqslant 0.99$. The transversal surface relaxivity ρ_2 was calculated from Eq. (1) for adsorbents that were equilibrated in water for 2 h. We used ρ_2 to scale T_2 time constants to pore size assuming a cylindrical pore geometry. We calculated T_2 in Eq. (1) as the mean time constant of the three-exponential fit (Eq. (2)) obtained after weighing each time constant by its fraction F_i. The bulk relaxa-

tion time T_{2b} of water is usually around 2.5 s and can thus be neglected to calculate ρ_2 from Eq. (1).

2.5. Differential scanning calorimetry

In order to characterize the state of water in PGA-coated alumina samples, we studied the freezing and melting of water using DSC analysis. Triplicate or quadruplicate samples of PGA-coated alumina (5–10 mg) that had been equilibrated for 2 and 170 h at 20 °C were weighed into standard Al pans, which were sealed hermetically prior to the DSC experiment. Differential scanning calorimetry experiments were performed with a DSC Q1000 (TA Instruments, Germany). The samples were abruptly cooled in the DSC instrument to −80 °C and then heated with 10 K min^{-1} from −80 to 110 °C, followed by a second abrupt cooling and subsequent heating cycle. In the cooling cycles, the freezing temperature (−20 °C) was reached within a maximum of 10 min, and the low temperature limit (−80 °C) was reached within 20 min. Nitrogen was employed as a purge gas. Baseline was corrected with the TZero technology® by TA instruments.

DSC data were analyzed using Universal Analysis software Version 4.1 (TA Instruments). The glass transition is indicated by an inflection point in the thermogram. Operationally, three tangent lines were applied for the evaluation, and the glass transition temperature (T_g) is defined as the temperature at the half-width of the central tangent line. The change of heat capacity (ΔC_p, J g^{-1} K^{-1}) was calculated from the height of the central tangent line. The amount of freezable and non-freezable water was determined by analyzing the endothermic melting peak between −11 °C and 27 °C. The transformation energy E (J g^{-1}) due to melting was calculated by integration of the peak using a linear baseline, and compared with the differential heat of fusion for free water ($H_{fus} = 333.5$ J g^{-1}, Ping et al., 2001) to estimate the amount of freezable and non-freezable water. Standard errors of freezable and non-freezable water were calculated from the standard error of the transformation energy E and the gravimetric water content of the samples, respectively. In order to determine the gravimetric water content of each individual sample, the Al pans were perforated after DSC analysis and dried at 105 °C for 6 h. The water content was then calculated from the weight difference before DSC measurement and after drying.

To calculate the means of T_g and ΔC_p, each subsample was analyzed eight times in order to minimize the nonsystematic error of data evaluation. The means of the glass transition temperature T_g, change in heat capacity ΔC_p, freezable and non-freezable water obtained for the two different equilibration times were compared using the unpaired t-test.

2.6. Phosphate sorption kinetics

Triplicate water-saturated samples with a mass equivalent to 0.625 g (dry weight) of pure or PGA-coated alumina were weighed into 2-L HD-PE bottles that were coated with Al-foil to exclude light. Subsequently, 250 mL of background electrolyte (0.01 M KNO_3, pH 5) were added before the samples were shaken on a horizontal shaker for 1 h at 150 rev min^{-1}. After pre-equilibration of the adsorbents, 1 L of background electrolyte solution was added containing 500 μM phosphate (as KH_2PO_4 p.a., Merck) and 5 μM $AgNO_3$ to impair microbial activity. The final phosphate concentration amounted to 400 μM (0.8 mmol P g^{-1} alumina). The pH was manually maintained at 5 ± 0.05 using dilute HNO_3 or KOH. After 0.5, 1, 2, 4, 8, 24, 48, 120, 144, and 168 h a 10-mL aliquot was removed from each subsample and 0.45-μm membrane filtered (polyethersulfone, Pall Life Science Supor®-450). The desorption of PGA-C was assessed by measuring total organic C in the 0.45-μm filtrates (Shimadzu TOC-5050A Autoanalyzer). A 2.5-mL aliquot of the 0.45-μm filtrate was ultracentrifuged at 440,000g for 1 h and phosphate was measured photometrically at 710 nm in the supernatant using the ascorbic–molybdenum blue method of Murphy and Riley (1962). The analytical precision of the photometric determination of phosphate was <1%. Subsample variability was generally <1.5%. Preliminary tests showed that matrix interferences of phosphate with polyvalent cations bound in the PGA structure did not occur during ultracentrifugation, i.e., phosphate concentrations in solution did not decrease due to sedimentation of PGA during ultracentrifugation.

The amount of phosphate sorbed was corrected for the water content of the samples (13 ± 1%), which was determined by outgassing the samples in an automated Autosorb-1 gas sorption system (Quantachrome, Syosset, NY) until the rate of pressure increase due to vapor evolution was below about 1.3 Pa min^{-1} within a 0.5-min test interval. Outgassing at elevated temperatures was not performed in order to avoid thermal transformations of PGA or the loss of chemisorbed water.

The phosphate sorption data were fitted with a linear combination of a modified first-order rate equation and the parabolic rate law (Crank, 1976) in order to account for the fast sorption to external alumina surfaces and the slow diffusion-controlled sorption of phosphate to alumina (Lang and Kaupenjohann, 2003; Mikutta et al., 2006a,b)

$$q_t = c_m - a_0 e^{-kt} + bt^{0.5}, \quad (3)$$

where q_t is the amount of phosphate sorbed at time t (μmol g^{-1}), c_m is the maximum amount of phosphate sorbed by the fast reaction (μmol g^{-1}), ($c_m - a_0$) is the amount of phosphate operationally defined as 'sorbed instantaneously' (μmol g^{-1}), i.e., at times ≪0.5 h, k is the rate constant of the fast phosphate sorption (h^{-1}), t is time (h), and b is the apparent rate constant of the slow sorption (μmol g^{-1} $h^{-0.5}$). The parameters c_m, a_0, k, and b were determined by minimizing the sum of the squared differences between the observed and predicted values of the phosphate sorption data using the Marquardt–Levenberg algorithm implemented in SigmaPlot 7.0 for Windows (SPSS Inc.).

The rate constant of the slow phosphate sorption, b, is related to the apparent diffusion constant $(D/r^2)_{app}$ (h^{-1})

$$b = 4q_\infty \pi^{-0.5}(D/r^2)_{app}^{0.5}, \quad (4)$$

where q_∞ is the amount of phosphate diffused at infinite time (μmol g^{-1}), D is the apparent diffusion coefficient (m^2 h^{-1}), and r is the radius of diffusion (m). We used the total amount of phosphate present at $t = 0$ h (μmol g^{-1}) corrected for the total amount of phosphate sorbed to external surfaces (c_m) as an approximation for q_∞ in Eq. (4) to calculate the apparent diffusion constant $(D/r^2)_{app}$.

3. Results and discussion

3.1. SEM analysis

Fig. 1 depicts SEM images of pure and PGA-coated alumina. Particles of the pure oxide possessed feather-edged structures that, when further resolved, showed a cauliflower-like surface microtopography with pore entrances of about 5 nm (image 5). The cauliflower-like surface structure shown in the high-resolution SEM image 5 (Fig. 1) is likely due to Au isles formed during sputtering. Similar structures have been observed on surfaces of layer silicates like pyrophyllite or vermiculite (not shown). Coatings of PGA greatly modified the microtopographical features of alumina. They comprised dense networks on external alumina surfaces that 'smoothed' the sharp edges of particle surfaces. Images 6–8 of Fig. 1 reveal that PGA polymers formed three-dimensional networks of interlacing fibrils having a length of up to several hundreds of nanometers. Aggregation of several PGA chains to larger fibrils in aqueous solution has been deduced from molecular dynamics calculations (Manunza et al., 1997). The nesting of PGA fibrils that existed as simple or multiple strands created new pores; the size of which varied considerably, ranging from less than 10 nm to several hundred nanometers (image 7 and 8). Similar structures have been reported for Ca-polygalacturonate coatings on garlic roots (Gessa and Deiana, 1992).

3.2. Porosity changes upon hydration

The C contents of PGA-coated alumina were stable upon equilibration in doubly deionized water for 1 week, showing that microbial activity was effectively reduced (Table 1). Porosity data obtained by N_2 gas adsorption at 77 K are presented in Table 1 and Fig. 2. Data in Table 1 indicate that PGA sorption to alumina hardly affected specific surface area, total pore volume, and micropore volume.

The BJH pore size distributions of both adsorbents obtained after equilibration in water for 2 and 170 h showed a monomodal distribution with a large peak at ~3 nm (Fig. 2). Judged on the pore size distribution of freeze-dried samples, no obvious difference existed between either pure and PGA-coated alumina and samples that had been equilibrated for 2 and 170 h, respectively (Fig. 2).

Complementary to the BJH pore size distribution of freeze-dried samples, Fig. 3 depicts the time constant distribution of water-saturated samples obtained from NMR relaxometry experiments. Each peak in Fig. 3 reflects a pore water domain or state of water binding in pores of varying size. The intensities are proportional to the amount of protons of water molecules relaxing with a defined time constant. The time constants of pure and PGA-coated alumina samples showed a bimodal distribution as identified from the magnetization decay curves using the regularization technique implemented in WinDXP software. Accordingly, one peak belonged to time constants <10 ms. The maximum of the major peak occurred between 55 and 100 ms for both adsorbents.

We calculated the mean transversal surface relaxivity ρ_2 for pure and PGA-coated alumina in order to assign peaks in Fig. 3 to either intra- or interparticle pores. The mean transversal surface relaxivity ρ_2 was 0.125 ± 0.011 nm ms^{-1} for pure alumina, and 0.169 ± 0.057 nm ms^{-1} for PGA-coated alumina (mean ± standard error). The ρ_2 parameters are at the lower end of published values. For example, D'Orazio et al. (1989) found values between 0.11 and 1.09 nm ms^{-1} for porous silica glass, and Mikutta et al. (2004) obtained 0.363 nm ms^{-1} for a hydrous Al oxide (γ-AlOOH). Differences in surface relaxivity among different types of minerals are mainly caused by differing physico-chemical properties of the materials (Hinedi et al., 1993). Based on ρ_2, a time constant of 10 ms (approximately middle between both peaks in Fig. 3) is equivalent to a pore size of about 5 nm assuming a cylindrical pore geometry. Therefore, the <10-nm peaks in Fig. 3 accord well with the pore size maximum of the BJH pore size distributions (Fig. 2), and can be attributed to intraparticle porosity. The 55–100-ms peaks are consequently attributed to water held in interparticle voids.

Fig. 3 shows that PGA sorption caused a redistribution of water in alumina samples; the amount of water held in intraparticle pores decreased concomitantly with an increase in the intensity of water held in larger pores. The decrease in water held in intraparticle alumina pores due to PGA sorption is shown by a statistically significant decrease in the sum of intensities below the <10-nm peaks of pure alumina after PGA sorption, independent of the equilibration time of the samples in water (Fig. 3, unpaired t-test, $P < 0.01$). We attribute the decrease in water content held in intraparticle pores to the displacement of pore water by PGA molecules. The incorporation of low- and high-molecular-weight amino acids into mesopores of silica and alumina has been proposed by Zimmerman et al. (2004a,b). However, pore size changes upon sorption of PGA to alumina were hardly detectable when samples were freeze-dried (Fig. 2). For PGA-coated samples, the 55–100-ms peaks consist of a mixture of mineral interparticle pores and pores created by PGA coatings. It should be noted that under moist conditions, PGA does probably not contain

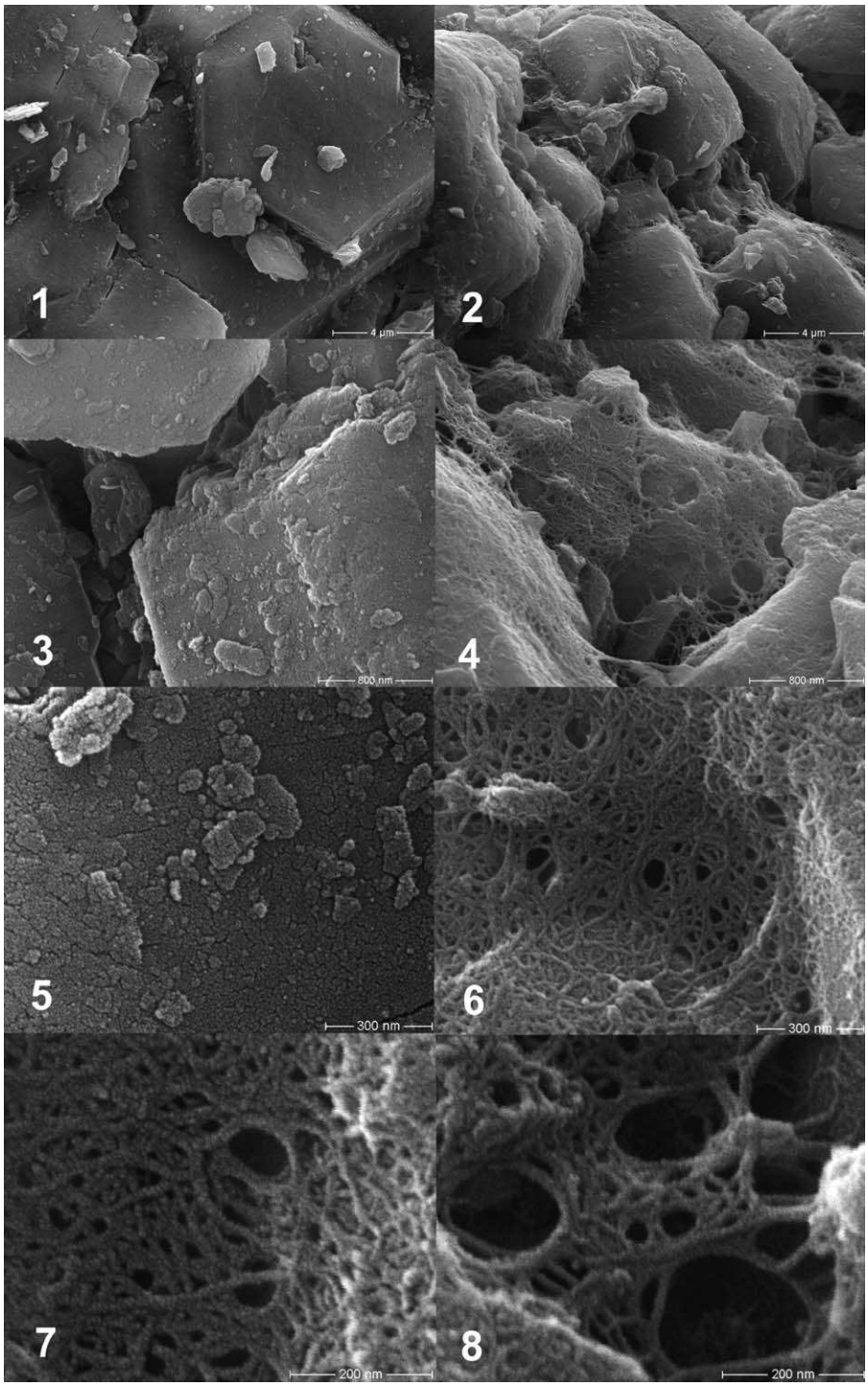

Fig. 1. Scanning electron microscopy images of pure (1, 3, and 5) and PGA-coated alumina (2, 4, and 6–8). The magnification of these images was 7000× (1 + 2), 40,000× (3 + 4), 100,000× (5 + 6), and 200,000× (7 + 8). Note that images 1–6 allow a direct comparison between pure and PGA-coated alumina. Images were obtained under ultra-high vacuum.

pores according to IUPAC nomenclature, i.e., cavities of porous solids that are deeper than wide (Rouquerol et al., 1994). Rather, PGA 'pores' represent interspaces between single PGA strands. The increase in peak amplitude of the 55–100-nm peak upon PGA-sorption (Fig. 3) could be solely attributed to PGA pores when a water content of PGA coatings of $\geqslant$98 wt% is assumed. In the presence of free water, root-cap mucilage can have water contents of up to 100,000% of its dry weight (Guinel and McCully, 1986). However, the water content reported for pure hydrogels is usually smaller than 98 wt% (Bajpai and Singh, 2006; Léveseque et al., 2005; Ruiz-Cabrera et al., 2005). Therefore, the difference between the major peak of pure and PGA-coated alumina samples (Fig. 3) is attrib-

Table 1
Carbon content, specific surface area (SSA) and pore characteristics of pure and PGA-coated alumina as determined with N_2 adsorption at 77 K

Treatment	Time elapsed before analysis (h)	C content (mg g^{-1})	SSA ($m^2 g^{-1}$)	Total pore volume ($mm^3 g^{-1}$)	D_p[a] (nm)	DR-Micropore volume ($mm^3 g^{-1}$)	Average micropore diameter (nm)
Al_2O_3	2	1.0 (0.1)	212 (2)	290 (5)	5.5 (0.1)	62 (1)	0.97 (0.01)
	170	0.8 (0.1)	215 (2)	293 (3)	5.5 (0.1)	65 (0)	0.97 (0.00)
Al_2O_3 + PGA	2	8.3 (0.6)	207 (1)	282 (1)	5.4 (0.1)	60 (1)	0.95 (0.00)
	170	8.4 (0.6)	213 (2)	275 (0)	5.2 (0.0)	63 (0)	0.93 (0.01)

Carbon contents are given as means obtained from C contents in the samples used for each experiment conducted (NMR, DSC, and phosphate sorption). Values in parentheses are given as standard errors.
[a] Average pore diameter.

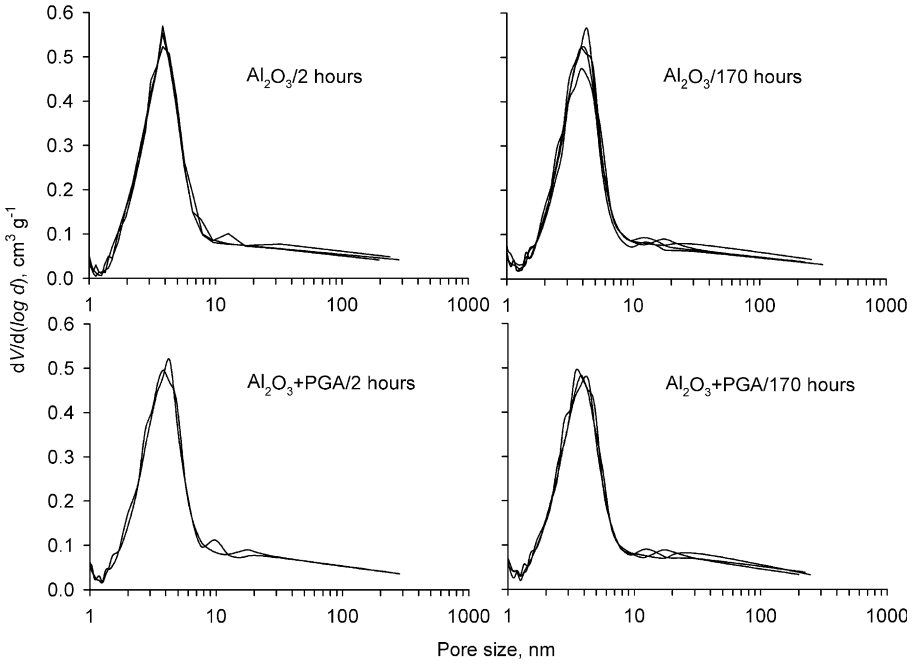

Fig. 2. Pore size distribution derived from the N_2 adsorption isotherm according to the BJH model (Barrett et al., 1951) of pure and PGA-coated alumina determined after 2 and 170 h of equilibration in doubly deionized water at 20 °C and pH 5. Before the N_2 adsorption measurements, the samples were frozen at −80 °C and freeze-dried. Note the log-scale of the *x*-axis.

uted to PGA pores and pores located at the PGA-alumina interface.

Our NMR results point at no significant porosity changes with time in moist PGA-coated alumina samples (Fig. 3), and thus accord with the N_2 adsorption results (Table 1, Fig. 2). Pores of PGA with widths of less than 100 nm (Fig. 1) were not detectable by N_2 adsorption at 77 K (Fig. 2) although they probably contributed significantly to the increase in amplitude of the 55–100-nm peak of PGA-coated alumina (Fig. 3). Dehydration of PGA-coatings upon freeze-drying probably led to conditions where the volume between interlacing PGA fibrils adds insignificantly to the total N_2-porosity of alumina particles. A collapse of pores created by PGA in interparticle pores of a hydrous Al oxide has been proposed by Mikutta et al. (2004). Because the distribution of water in a sample is a prerequisite for solute transport from the bulk water phase into intraparticle pores, porosities obtained on dehydrated organic matter-coated specimens using gas adsorption may not adequately reflect the 'effective' pore size distribution.

3.3. Differential scanning calorimetry

Fig. 4 shows representative DSC thermograms of the PGA-coated alumina after 2 and 170 h of equilibration in water, respectively. Both thermograms are comparable in shape and show a step transition between −50 and −20 °C followed by an endothermic peak with a maximum between 4 and 6 °C. In accordance to findings for gelatine gels (Nishinari et al., 1997), starch gels (Tananuwong and Reid, 2004) and water–gellan systems (Hatakeyama et al., 1999), we interpret the step transition as glass transition of the solidified amorphous gel matrix, and the endotherm was attributed to melting of frozen water.

The shape of DSC thermograms of hydrogels is generally explained as follows: Various kinds of hydrogels form glassy matrixes by quenching to low temperatures (Nishi-

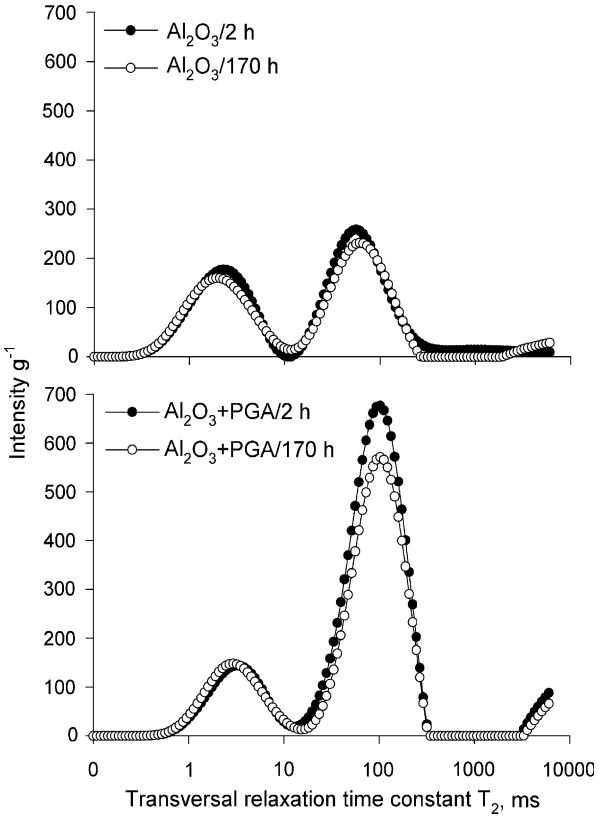

Fig. 3. Transversal relaxation time constant (T_2) distributions of pure and PGA-coated alumina obtained after 2 and 170 h of equilibration in doubly deionized water at 20 °C and pH 5. For the sake of clarity only the results for one replicate sample are presented. Differences in peak amplitudes among replicate samples shown are not statistically significant at $P = 0.05$. Relaxation time constant distributions were highly reproducible in replicate samples of each treatment (not shown). The distributions were normalized to the mass of alumina in the samples. Note the log-scale of the x-axis.

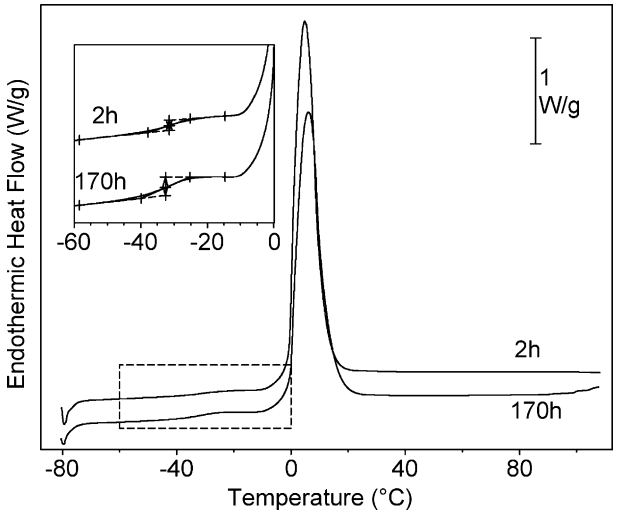

Fig. 4. Differential scanning calorimetry thermograms of the PGA-coated alumina after 2 and 170 h of equilibration in doubly deionized water at 20 °C and pH 5. For better visualization graphs are stacked. The inset shows the expanded view of the glass transition region.

nari et al., 1997). During cooling of hydrogels, ice crystallization can occur only before the matrix becomes glassy. A part of the water molecules associated closely with the polymers solidifies in an amorphous state (Nishinari et al., 1997). The system is then separated into an ice phase and an unfrozen phase, which results in many small, discrete ice crystals embedded in a continuous, rubbery phase of freeze-concentrated polymer and unfrozen water. At a sufficiently low temperature, this unfrozen phase solidifies into a glassy state, and ice formation ceases because of kinetic restrictions, although a certain amount of water still remains unfrozen. The unfrozen water in the amorphous phase has been proposed to be associated in some way closely with the solute molecules, although it may not totally be immobilized or "bound" (Tananuwong and Reid, 2004). By heating during the DSC experiment, the amorphous ice (which is associated with the matrix) becomes mobile, and the increase in mobility expresses as glass transition at T_g (Nishinari et al., 1997), while melting of the ice crystallites is expressed by the endothermic peak above T_g. The glass transition temperature decreases with increasing content of unfrozen water in the low-water-content region of hydrogels (Nishinari et al., 1997; Hatakeyama et al., 1999). This decrease is explained with the plasticizing effect of water (Hatakeyama et al., 1999). The change of heat capacity, ΔC_p, is a measure for the quantity of the amorphous phase, which is related to the amount of unfrozen water. An increase of ΔC_p is thus connected with a decrease in the glass transition temperature (T_g). T_g re-increases in the higher water-content region due to increasing restrictions of the polymer mobility around ice crystallites (Hatakeyama et al., 1999). The quantity and the restriction of the glassy amorphous phase is in this case directly related to the total surface of the ice crystallites, and thus, both T_g and ΔC_p increase with increasing amount of frozen water.

Table 2 summarizes the melting and glass transition characteristics of the PGA-coated alumina for the two equilibration times. The samples revealed water contents of 58% with a standard error of 4% (total mass basis); differences between the equilibration times were not significant. While the glass transition temperature decreased significantly from −31.9 to −33.4 °C with equilibration time, ΔC_p showed a significant increase from 0.26 to 0.38 J $g^{-1}K^{-1}$. This indicates that the system behaves like low-water-content gels, in which water acts as plasticizer, i.e., increases the content of more rubbery gel domains. The change in heat capacity, ΔC_p, is a direct measure for the quantity of an amorphous phase. The increase of ΔC_p thus indicates an increase of the amorphous (gel) phase with equilibration time. This conclusion is in accordance with the observation that ΔC_p is slightly higher in fully gelatinized gels than in partly gelatinized gels (Tananuwong and Reid, 2004). The lower T_g suggests that PGA molecules became more flexible after 170 h of equilibration.

The area of the endotherm peaks indicates transformation energies E of 173 and 159 J g^{-1} for equilibration times

Table 2
Changes in T_g, ΔC_p, the energy of transformation E upon hydration of PGA-coated alumina for 2 and 170 h

Parameter	PGA-coated Al_2O_3 equilibrated for	
	2 h	170 h
T_g (°C)	−31.9 (0.4)	−33.4 (0.3)[a]
ΔC_p (J g^{-1} K^{-1})	0.26 (0.03)	0.38 (0.01)[a]
Transformation energy E (J g^{-1})	173 (6)	159 (5)NS
Freezable water (%)	52 (4)	46 (4)NS
Non-freezable water (%)	7 (6)	11 (6)NS

NS indicates nonsignificant differences between equilibration times on the $P = 0.05$ level. Water contents and transformation energy are related to the total sample mass. Also given are estimates of freezable and non-freezable water. Figures in parentheses denote standard error.

[a] Significant differences between equilibration times on the $P = 0.01$ probability level.

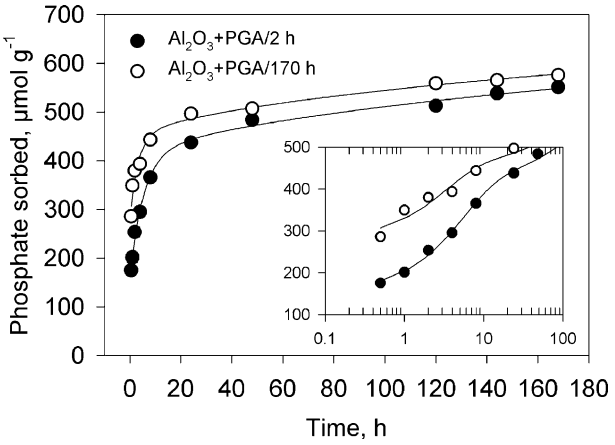

Fig. 5. Phosphate sorption kinetics of PGA-coated alumina after 2 and 170 h of equilibration in doubly deionized water at 20 °C, pH 5, $I = 0.01$ M, and an initial phosphate concentration of 400 µM. The solid concentration was 0.5 g L^{-1}. The inset shows the phosphate sorption of the first 100 h with a logarithmic x-axis. Error bars are smaller than the symbol size. Solid lines indicate model fits of Eq. (3).

of 2 and 170 h, respectively, which suggests a higher amount of unfrozen water after 170 h of equilibration (11%) than after 2 h of equilibration (7%). Although the differences were not significant on the $P = 0.05$ level, they show the tendency expected from the increase in ΔC_p and thus support the assumption that the amount of a gel phase increased during equilibration. For a final verification of this relation, the water contents of the individual samples need to be determined with higher accuracy. In summary, the DSC investigation suggests an increase in the flexibility of PGA molecules and the amount of a PGA gel phase, and most probably indicates a hydration-induced swelling of the PGA coatings.

3.4. Phosphate sorption kinetics

To test our initial hypothesis that restructuring of PGA sorbed to alumina affects the kinetics of phosphate immobilization, we conducted batch experiments after equilibrating both adsorbents in doubly deionized water for 2 and 170 h, respectively. The phosphate sorption to pure and PGA-coated alumina comprised a fast and a slow reaction as shown for the PGA-coated sample in Fig. 5. The fast initial sorption is attributed to sorption of phosphate to external, rapidly accessible sorption sites, while the slow phosphate sorption has been explained by diffusion of phosphate to internal sorption sites (Shin et al., 2004). The kinetic parameters obtained by fitting Eq. (3) to the phosphate sorption data are presented in Table 3. PGA-coatings reduced the total amount of phosphate immobilized by the fast sorption reaction and the amount of phosphate that was operationally defined as instantaneously sorbed (Table 3, c_m, $c_m - a_0$ for $t = 2$ h). The apparent diffusion constant, $(D/r^2)_{app}$, of pure alumina was 4.7×10^{-4} h^{-1} (Table 3). From this value, we estimated the apparent diffusion coefficient D_{app}. Because the radius of diffusion is probably much less than one-half of the particle's diameter (<105 µm), we arbitrarily chose a diffusion path length of 10 µm and calculated D_{app} with 1.1×10^{-12} m^2 day^{-1}. The D_{app} was seven orders of magnitude lower than the diffusion coefficient D_0 of $H_2PO_4^-$ in water at 25 °C (7.6×10^{-5} m^2 day^{-1}, Edwards and Huffman, 1959), showing that the diffusion of phosphate in intraparticle pores of alumina was considerably slowed down. However, parameters referring to the slow phosphate sorption remained unaffected by the PGA coating, which indicates that the diffusion of phosphate into intraparticle pores was not impaired by PGA (Table 3).

The phosphate sorption kinetics of pure alumina remained more or less unaffected by the pre-equilibration time (Table 3). In contrast, the phosphate sorption kinetics of PGA-coated alumina strongly depended on the duration of equilibration in water. The amount of phosphate being instantaneously sorbed ($c_m - a_0$) and the total amount of phosphate sorbed by the fast reaction (c_m) increased by 84% and 12%, respectively (Table 3). The result implies that after equilibration of PGA-coated samples for 170 h, external alumina surfaces became more accessible to phosphate. The phosphate sorption kinetics is in line with our DSC measurements showing that PGA molecules became more 'flexible' after 170 h of equilibration in doubly deionized water.

Although the swelling kinetics of soil organic matter represents a slow process with time constants varying between one and 6 days (Schaumann et al., 2004), the slow phosphate sorption to alumina remained unaffected by the state of sorbed organic matter (Table 3, b, $(D/r^2)_{app}$). One possible explanation is that structural changes of PGA molecules proceeded too fast to have a significant impact on the slow phosphate sorption. This reasoning accords with the finding that mucilage of maize plants, which comprises about 90–95% polysaccharides with 20–35% uronic acids (Cortez and Billes, 1982; Morel et al., 1986), swells within minutes due to water absorption (Guinel and McCully, 1986; Sealey et al., 1995; McCully

Table 3
Kinetic parameters obtained by fitting Eq. (3) to the phosphate sorption data of pure and PGA-coated alumina that had been equilibrated at pH 5 in doubly deionized water for 2 and 170 h, respectively, prior to phosphate sorption

Treatment	Time elapsed until P sorption (h)	c_m (μmol g^{-1})	$c_m - a_0$ (μmol g^{-1})	k (h^{-1})	b (μmol g^{-1} $h^{-0.5}$)	r^2	$(D/r^2)_{app}$ ($\times 10^{-4}$ h^{-1})
Al_2O_3	2	506 (22)	296 (31)	0.20 (0.05)	14.3 (2.1)	0.99	4.7 (0.9)
Al_2O_3	170	504 (38)	296 (53)	0.15 (0.06)	8.7 (3.7)	0.98	1.7 (1.0)
Al_2O_3 + PGA	2	383 (14)	150 (20)	0.19 (0.03)	12.8 (1.4)	1.00	1.8 (0.3)
Al_2O_3 + PGA	170	430 (21)	276 (31)	0.32 (0.12)	11.4 (2.1)	0.98	1.9 (0.5)

Parameter meaning: c_m, total amount of phosphate sorbed fast; $c_m - a_0$, operationally defined amount of phosphate sorbed instantaneously; k, rate constant of the fast reaction; b, rate constant of the slow phosphate sorption; $(D/r^2)_{app}$, apparent diffusion constant according Eq. (4). Values in parentheses indicate standard error.

and Sealey, 1996). Another explanation for the lacking effect on structural changes of PGA on the slow phosphate sorption kinetics is that after 2 h of equilibration in water, PGA desorption was so fast that structural changes of the remaining PGA at the alumina surface did not affect the slow phosphate sorption. Indeed, during the first 0.5 h after phosphate addition 68% of the total desorbed PGA-C were desorbed (Fig. 6).

Another line of evidence indicating a decrease in PGA surface coverage with increasing equilibration time comes from Fig. 6, showing the relationship between the quantities of phosphate sorbed and PGA-C desorbed. Phosphate is highly competitive with pre-sorbed PGA (Mikutta et al., 2006a). During phosphate sorption to PGA-coated alumina for one week, phosphate displaced 54% and 41% of the initial PGA-C in samples that had been equilibrated for 2 and 170 h, respectively. The slopes of the linear regressions presented in Fig. 6 show that after a 2-h equilibration period each phosphate displaced on average 0.4 C atoms. The slope increased by a factor of 2 when the samples were equilibrated for 170 h before phosphate addition, indicating a higher efficacy of phosphate to desorb PGA-C in samples in which the PGA coating comprised more rubbery domains. In addition, Fig. 6 shows that a much larger portion of phosphate was required to achieve a significant C desorption in samples that had been equilibrated for 170 h. Contrary, although phosphate was less competitive with PGA-C in samples that were equilibrated for 2 h only, PGA-C desorption started at a lower phosphate surface loading in these samples (Fig. 6).

3.5. Conceptual model

In Fig. 7 we present a conceptual model for the experimental results of our DSC and phosphate sorption experiments. The picture shows a planar alumina surface coated with linear PGA polymers. The PGA polymers are shown as chains with each link representing a galacturonate monomer. Dark gray chain segments indicate monomers that are directly attached physically or chemically to the alumina surface. White spheres symbolize phosphate ions. Accordingly, after 2 h of equilibration in doubly deionized water, a larger fraction of PGA is sorbed in a comparatively flat conformation (poorly hydrated state, less flexible), in which PGA polymers are intimately attached to the mineral surface. Consequently, less sorption sites are rapidly accessible to phosphate (Table 3, $c_m - a_0$) and phosphate is less able to displace a PGA molecule from the surface

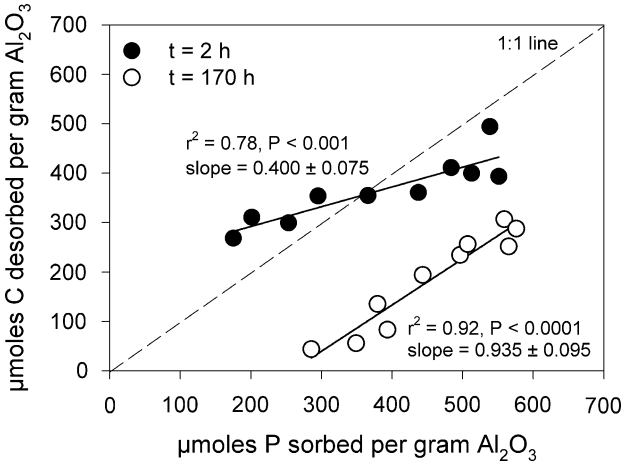

Fig. 6. Plot of the amount of phosphate sorbed versus PGA-C desorbed during 1 week of phosphate sorption to PGA-coated alumina at pH 5 in 0.01 M KNO_3 with an initial phosphate concentration of 400 μM and a solid concentration of 0.5 g L^{-1}.

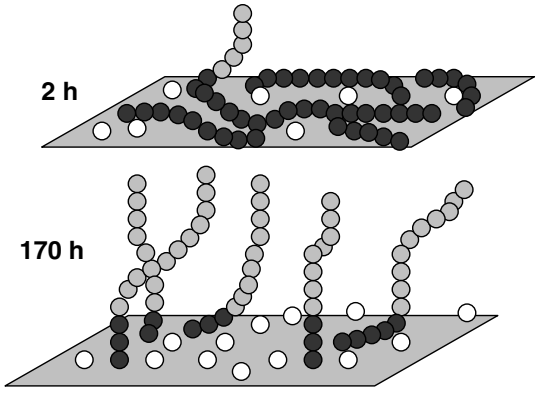

Fig. 7. Conceptual model of the dynamics of PGA ions at the alumina surface at pH 5 and $I = 0.01$ M, and its consequences for phosphate sorption and PGA desorption. Gray spheres indicate chain segments of PGA (galacturonic acid monomers): dark gray, monomers linked to the surface; light gray, unbound chain segments with respect to the alumina surface; white spheres symbolize phosphate ions. For explanations, please refer to Section 3.5.

('octopus' effect, Podoll et al., 1987; see Fig. 6). Based on the high competitiveness of phosphate with pre-sorbed PGA (Mikutta et al., 2006a), a lower phosphate loading is required after 2 h to induce PGA desorption.

After equilibration of PGA-coated alumina for 170 h, in water PGA molecules rearrange and the mobility of polymer chains increases (swollen state, more flexible). This process decreases the surface coverage of alumina by PGA and facilitates the diffusion of phosphate ions from the bulk water solution to external alumina surfaces (Table 3, c_m, $c_m - a_0$). Upon hydration, PGA polymers become less intimately associated with the mineral surface as indicated by less dark gray chain segments of PGA molecules after 170 h (Fig. 7). When the external surfaces reach saturation with phosphate ions, phosphate increasingly competes with sorbed PGA at higher phosphate surface loading. As the polymers are less intimately attached to the mineral surface, the efficacy of phosphate to displace PGA-C increases (Fig. 6).

Noteworthy, at a given phosphate loading more PGA-C is desorbed in samples that had been equilibrated for 2 h than for 170 h although the PGA-C seems to be less susceptible to desorption by phosphate in the 2-h treatment (Fig. 6). This observation probably results from a greater portion of weakly bound PGA in the 2 h treatment which is readily displaced by phosphate at times <0.5 h. In general, factors that need to be considered include (i) the average strength of PGA-oxide interaction which depends on the distribution of weak and strong bindings (e.g., electrostatic vs. specific interaction) of PGA segments to the alumina surface, (ii) the amount of free binding sites (type A-hydroxyls) remaining for specific interaction with phosphate after initial PGA sorption, (iii) the affinity of phosphate to the oxide surface relative to that of pre-sorbed PGA, and (iv) the destabilization of sorbed PGA polymers by locally increased negative surface charge of alumina imparted by phosphate. It is worth mentioning that the concept developed is oversimplified but following the rule of parsimony (Ockham's razor) it provides a reasonable explanation for our experimental results.

4. Summary and conclusions

Porosity studies with ^{1}H NMR and N_2 gas adsorption of moist and freeze-dried PGA-coated alumina, which had been equilibrated in water for 2 and 170 h, respectively, revealed no swelling-induced change in pore size. Our NMR measurements showed that water held in intraparticle pores of alumina was partially displaced by sorbed PGA. Additionally, the hydration of PGA networks on external alumina surfaces increased the amount of water held in interparticle pores of alumina–PGA associations, suggesting the formation of new intra-organic pores between alumina particles.

The analysis of the state of water binding in PGA-coated samples with DSC showed that within 168 h of equilibration in water the quantity of the PGA gel phase increased, indicating an increase in rubbery domains of the PGA coating. Accordingly, the accessibility of external sorption sites for phosphate was larger after 170 h than after 2 h. The slow phosphate sorption to alumina was independent of equilibration time. The restructuring of sorbed polymers with time changed the efficacy of phosphate to desorb PGA. When PGA coatings became more flexible upon hydration for 170 h, PGA molecules were less intimately attached to the mineral surface. As a consequence, phosphate was more efficient in displacing PGA C. However, a higher surface loading of phosphate was required because more free binding sites existed on external alumina surfaces. We finally conclude that structural changes upon hydration/dehydration of plant- or microbe-derived macromolecules sorbed to minerals can be regarded as a crucial factor influencing sorption and transport phenomena of solutes in soils.

Acknowledgments

We thank Fabian Jaeger for useful discussions on the ^{1}H NMR results. We also thank Jeannette Regnery who kindly supported us in the DSC analysis. In addition, we thank three anonymous reviewers for their encouraging statements. This research was funded by the German Research Fund (DFG, KA 1139/8).

Associate editor: Carrick M. Eggleston

References

Allison, S.D., Randolph, T.W., Mannung, M.C., Middleton, K., Davis, A., Carpenter, J.F., 1998. Effect of drying methods and additives on structure and function of actin: mechanisms of dehydration-induced damage and its inhibition. *Arch. Biochem. Biophys.* **358**, 171–181.

Altfelder, S., Streck, T., Richter, J., 1999. Effect of air-drying on sorption kinetics of the herbicide chlortoluron in soil. *Environ. Qual.* **28**, 1154–1161.

Bajpai, S.K., Singh, S., 2006. Analysis of swelling behavior of poly(methacrylamide-co-methacrylic acid) hydrogels and effect of synthesis conditions on water uptake. *Reactive and Functional Polymers* **66**, 431–440.

Barrett, E.P., Joyner, L.G., Halenda, P.P., 1951. The determination of pore volume and area distributions in porous substances. I. Computations from nitrogen isotherms. *J. Am. Chem. Soc.* **73**, 373–380.

Brownstein, K.R., Tarr, C.E., 1979. Importance of classical diffusion in NMR studies of water in biological cells. *Phys. Rev. A* **19**, 2446–2453.

Brunauer, S., Emmett, P.H., Teller, E., 1938. Adsorption of gases in multimolecular layers. *J. Am. Chem. Soc.* **60**, 309–319.

Brusseau, M., Rao, P.S.C., 1989. Sorption nonideality during organic contaminant transport in porous media. *Crit. Rev. Environ. Control* **19**, 33–99.

Cornelissen, G., van Noort, P.C.M., Govers, H.A.J., 1998. Mechanisms of slow desorption of organic compounds from sediments: A study using model sorbents. *Environ. Sci. Technol.* **32**, 3124–3131.

Cortez, J., Billes, G., 1982. Rôle des ions calcium dans la formation du mucigel de Zea mays. *Acta Oecol. Plant.* **3**, 67–78.

Crank, J., 1976. *The Mathematics of Diffusion*. Oxford University Press, New York.

D'Orazio, F., Tarczon, J.C., Halperin, W.P., Eguchi, K., Mizusaki, T., 1989. Application of nuclear magnetic resonance pore structure analysis to porous silica glass. *J. Appl. Phys.* **65**, 742–751.

Edwards, O.W., Huffman, E.O., 1959. Diffusion of aqueous solutions of phosphoric acid at 25°. *J. Phys. Chem.* **63**, 1830–1833.

Gaillardon, P., 1996. Influence of soil moisture on long-term sorption of diuron and isoproturon by soil. *Pestic. Sci.* **47**, 347–354.

Gerin, P.A., Genet, M.J., Herbillon, A.J., Delvaux, B., 2003. Surface analysis of soil material by X-ray photoelectron spectroscopy. *Eur. J. Soil Sci.* **54**, 589–603.

Gessa, C., Deiana, S., 1992. Ca-polygalacturonate as a model substance for a soil–root interface. II. Fibrillar structure and comparison with natural root mucilage. *Plant soil* **140**, 1–13.

Gregg, S.J., Sing, K.S.W., 1982. *Adsorption, Surface Area and Porosity*. Academic Press, New York.

Guinel, F.C., McCully, M.E., 1986. Some water-related physical properties of maize root-cap mucilage. *Plant Cell Environ.* **9**, 657–666.

Hatakeyama, T., Nakamura, K., Takahashi, M., Hatakeyama, H., 1999. Phase transitions of gellan-water systems. *Prog. Coll. Pol. Sci.* **114**, 98–101.

Heil, D., Sposito, G., 1995. Organic matter role in illitic soil colloids flocculation: III. Scanning force microscopy. *Soil Sci. Soc. Am. J.* **59**, 266–269.

Hinedi, Z.R., Kabala, Z.J., Skaggs, T.H., Borchardt, D.B., Lee, R.W.K., Chang, A.C., 1993. Probing soil and aquifer material porosity with nuclear magnetic resonance. *Water Resour. Res.* **29**, 3861–3866.

Hinedi, Z.R., Chang, A.C., Anderson, M.A., Borchardt, D.B., 1997. Quantification of microporosity by nuclear magnetic resonance relaxation of water imbibed in porous media. *Water Resour. Res.* **33**, 2697–2704.

Johnson, A.C., Bettinson, R.J., Williams, R.J., 1999. Differentiating between physical and chemical constraints on pesticide and water movement into and out of soil aggregates. *Pestic. Sci.* **55**, 524–530.

Jouppila, K., Roos, Y.H., 1997. The physical state of amorphous corn starch and its impact on crystallization. *Carbohydr. Polymers* **32**, 95–104.

Kaiser, K., Guggenberger, G., 2003. Mineral surfaces and soil organic matter. *Eur. J. Soil Sci.* **54**, 219–236.

Kenyon, W.E., 1992. Nuclear magnetic resonance as a petrophysical measurement tool. *Nucl. Geophysics* **6**, 153–171.

Kenyon, W.E., 1997. Petrophysical principles of applications of NMR logging. *Log Analyst* **38**, 21–46.

Knee, E.M., Gong, F.-C., Gao, M., Teplitski, M., Jones, A.R., Foxworthy, A., Mort, A.J., Bauer, W.D., 2001. Root mucilage from pea and its utilization by rhizosphere bacteria as a sole carbon source. *Mol. Plant Microbe. Interact.* **14**, 775–784.

Lang, F., Kaupenjohann, M., 2003. Immobilisation of molybdate by iron oxides: effect of organic coatings. *Geoderma* **113**, 31–46.

LeBoeuf, E.J., Weber Jr., W.J., 1997. A distributed reactivity model for sorption by soils and sediments. 8. Sorbent organic domains: discovery of a humic acid glass transition and an argument for a polymer-based model. *Environ. Sci. Technol.* **31**, 1697–1702.

LeBoeuf, E.J., Weber Jr., W.J., 2000. Macromolecular characteristics of natural organic matter. 2. Sorption and desorption behavior. *Environ. Sci. Technol.* **34**, 3623–3631.

Léveseque, S.G., Lim, R.M., Shoichet, M.S., 2005. Macroporous interconnected dextran scaffolds controlled porosity for tissue-engineering applications. *Biomaterials* **26**, 7436–7446.

Manunza, B., Deiana, S., Pintore, M., Gessa, C., 1997. Molecular dynamics study of polygalacturonic acid chains in aqueous solution. *Carbohydr. Res.* **300**, 85–88.

Mayer, L.M., Xing, B., 2001. Organic matter-surface area relationships in acid soils. *Soil. Sci. Soc. Am. J.* **65**, 250–258.

McCully, M.E., Sealey, L.J., 1996. The expansion of maize root-cap mucilage during hydration. 2. Observations on soil-grown roots by cryo-scanning electron microscopy. *Physiol. Plant.* **97**, 454–462.

Mikutta, C., Lang, F., Kaupenjohann, M., 2004. Soil organic matter clogs mineral pores: evidence from ^{1}H-NMR logging and N_2 adsorption. *Soil Sci. Soc. Am. J.* **68**, 1853–1862.

Mikutta, C., Lang, F., Kaupenjohann, M., 2006a. Kinetics of phosphate sorption to polygalacturonate-coated goethite. *Soil Sci. Soc. Am. J.* **70**, 541–549.

Mikutta, C., Lang, F., Kaupenjohann, M., 2006b. Citrate impairs the micropore diffusion of phosphate into pure and C-coated goethite. *Geochim. Cosmochim. Acta* **70**, 595–607.

Morel, J.L., Mench, M., Guckert, A., 1986. Measurement of Pb^{2+}, Cu^{2+} and Cd^{2+} binding with mucilage exudates from maize (*Zea mays L.*) roots. *Biol. Fertil. Soils* **2**, 29–34.

Murphy, J., Riley, J.P., 1962. A modified single solution method for determination of phosphate in natural waters. *Anal. Chim. Acta* **26**, 31–36.

Nishinari, K., Watase, M., Hatakeyama, T., 1997. Effects of polyols and sugars on the structure of water in concentrated gelatin gels as studied by low temperature differential scanning calorimetry. *Colloid Polymer Sci.* **275**, 1078–1082.

Pignatello, J.J., Xing, B., 1996. Mechanisms of slow sorption of organic chemicals to natural particles. *Environ. Sci. Technol.* **30**, 1–11.

Ping, Z.H., Nguyen, Q.T., Chen, S.M., Zhou, J.Q., Ding, Y.D., 2001. States of water in different hydrophilic polymers—DSC and FTIR studies. *Polymer* **42**, 8461–8467.

Podoll, R.T., Irwin, K.C., Brendlinger, S., 1987. Sorption of water-soluble oligomers on sediments. *Environ. Sci. Technol.* **21**, 562–568.

Ransom, B., Bennet, R.H., Baerwald, R., Shea, K., 1997. TEM study of in situ organic matter on continental margins: occurrence of the 'monolayer' hypothesis. *Marine Geol.* **138**, 1–9.

Rouquerol, J., Avnir, D., Fairbridge, C.W., Everett, D.H., Haynes, J.H., Pernicone, N., Ramsay, J.D.F., Sing, K.S.W., Unger, K.K., 1994. Recommendations for the characterization of porous solids. *Pure Appl. Chem.* **66**, 1739–1758.

Rovira, A.D., 1969. Diffusion of carbon compounds away from wheat root. *Aust. J. Biol. Sci.* **22**, 1287–1290.

Ruiz-Cabrera, M.A., Foucat, L., Bonny, J.M., Renou, J.P., Daudin, J.D., 2005. Assessment of water diffusivity in gelatine gel from moisture profiles. II. Data processing adapted to material shrinkage. *J. Food Eng.* **68**, 221–231.

Schaumann, G.E., 2005. Matrix relaxation and change of water state during hydration of peat. *Colloids Surfaces A* **265**, 163–170.

Schaumann, G.E., LeBoeuf, E.J., 2005. Glass transitions in peat: their relevance and the impact of water. *Environ. Sci. Technol.* **39**, 800–806.

Schaumann, G.E., Antelmann, O., 2000. Thermal characteristics of soil organic matter measured by DSC: a hint on a glass transition. *J. Plant Nutr. Soil Sci.* **163**, 179–181.

Schaumann, G.E., Sievert, C., Marschner, B., 2000. Kinetics of the release of dissolved organic matter (DOM) from air-dried and pre-moistened soil material. *J. Plant Nutr. Soil Sci.* **163**, 1–5.

Schaumann, G.E., Hurraß, J., Müller, M., Rotard, W., 2004. Swelling of organic matter in soil and peat samples: insights from proton relaxation, water absorption and PAH extraction. In: Ghabbour, E.A., Davies, G. (Eds.), *Humic Substances: Nature's Most Versatile Materials*. Taylor and Francis Inc, New York, pp. 101–117.

Schaumann, G.E., Hobley, E., Hurraß, J., Rotard, W., 2005. H-NMR Relaxometry to monitor wetting and swelling kinetics in high-organic matter soils. *Plant. Soil* **275**, 1–20.

Sealey, I.J., McCully, M.E., Canny, M.J., 1995. The expansion of maize root-cap mucilage during hydration. 1. *Kinet. Physiol. Plant.* **93**, 38–46.

Shin, E.W., Han, J.S., Jang, M., Min, S.-H., Park, J.K., Rowell, R.M., 2004. Phosphate adsorption on aluminum-impregnated mesoporous silicates: surface structure and behaviour of adsorbents. *Environ. Sci. Technol.* **38**, 912–917.

Souillac, P.O., Middaugh, C.R., Rytting, J.H., 2002. Investigation of protein/carbohydrate interactions in the dried state. 2. Diffuse relectance FTIR studies. *Int. J. Pharm.* **235**, 207–218.

Straley, C., Rossini, D., Vinegar, H., Tutunjian, P., Morris, C., 1997. Core analysis by low field NMR. *Log Analyst* **38**, 84–94.

Tananuwong, K., Reid, D.S., 2004. Differential scanning calorimetry study of glass transition in frozen starch gels. *J. Agric. Food Chem.* **52**, 4308–4317.

Wedlock, D.J., Philips, G.O., Davies, A., Gormally, J., Wyn-Jones, E., 1983. Depolymerization of sodium hyaluronate during freeze drying. *Int. J. Biol. Macromol.* **5**, 186–188.

Young, R.J., Lovell, P.A., 1991. *An Introduction to Polymers*. Chapman & Hall, London.

Zimmerman, A.R., Goyne, K.W., Chorover, J., Komarneni, S., Brantley, S.L., 2004a. Mineral mesopore effects on nitrogenous organic matter adsorption. *Org. Geochem.* **35**, 355–375.

Zimmerman, A.R., Chorover, J., Goyne, K.W., Brantley, S.L., 2004b. Protection of mesopore-adsorbed organic matter from enzymatic degradation. *Environ. Sci. Technol.* **38**, 4542–4548.

View publication stats